


SCIENTIFIC REPORTS



OPEN

Genetic elimination of dopamine vesicular stocks in the nigrostriatal pathway replicates Parkinson's disease motor symptoms without neuronal degeneration in adult mice

Elsa Isingrini¹, Chloé Guinaudie¹, Léa C Perret¹, Quentin Rainer¹, Luc Moquin¹, Alain Gratton¹ & Bruno Giros^{1,2} 

The type 2 vesicular monoamine transporter (VMAT2), by regulating the storage of monoamines transmitters into synaptic vesicles, has a protective role against their cytoplasmic toxicity. Increasing evidence suggests that impairment of VMAT2 neuroprotection contributes to the pathogenesis of Parkinson's disease (PD). Several transgenic VMAT2 mice models have been developed, however these models lack specificity regarding the monoaminergic system targeting. To circumvent this limitation, we created VMAT2-KO mice specific to the dopamine (DA) nigrostriatal pathway to analyze VMAT2's involvement in DA depletion-induced motor features associated to PD and examine the relevance of DA toxicity in the pathogenesis of neurodegeneration. Adult VMAT2 floxed mice were injected in the substantia nigra (SN) with an adeno-associated virus (AAV) expressing the Cre-recombinase allowing VMAT2 removal in DA neurons of the nigrostriatal pathway solely. VMAT2 deletion in the SN induced both DA depletion exclusively in the dorsal striatum and motor dysfunction. At 16 weeks post-injection, motor symptoms were accompanied with a decreased in food and water consumption and weight loss. However, despite an accelerating death, degeneration of nigrostriatal neurons was not observed in this model during this time frame. This study highlights a non-cytotoxic role of DA in our genetic model of VMAT2 deletion exclusively in nigrostriatal neurons.

Parkinson's disease (PD), is one of the most common neurodegenerative disorders affecting 1–2% of individuals older than 65 years old worldwide¹. PD is a progressive disorder clinically characterized by a large number of motor features in particular rest tremor, bradykinesia, rigidity and loss of postural reflexes^{2,3}. At the pathological level, processes leading to PD begin before the appearance of the typical motor symptoms, and by the time the disease is diagnosed about 70–80% of striatal dopamine (DA) is depleted and one third of substantia nigra (SN) DA neurons and striatal DA fibers are already lost^{2,4–7}. Understanding the biochemical markers relevant to the pathogenesis of neurodegeneration in PD remain essential.

Oxidative stress contribution to PD neurodegeneration is currently well established⁸. Post-mortem studies have shown an imbalance between reactive oxygen species (ROS) production and the antioxidant protective system resulting in oxidative stress in the SN of PD patients^{9,10}. Superoxide (O_2^-), hydrogen peroxide (H_2O_2), and the hydroxyl radical ($OH\cdot$), three important ROS in mammalian cells, can damage macromolecules including nucleic acids, lipids and proteins, leading to DA neuron degeneration, and neuron network dysfunction, ultimately progressing to PD¹¹. For a better understanding of the oxidative stress mechanisms in PD, the MPTP

¹Department of Psychiatry, Douglas Mental Health Research Center, McGill University, Montreal, Quebec, H4H 1R3, Canada. ²Sorbonne Universités, Neuroscience Paris Seine, CNRS UMR 8246, INSERM U 1130, UPMC Univ Paris 06, UM119, 75005, Paris, France. Correspondence and requests for materials should be addressed to B.G. (email: bruno.giros@mcgill.ca)

(1-méthyl-4-phényl-1,2,3,6-tétrahydropyridine) model is currently used. MPTP's metabolite MPP⁺, taken up by DA neurons inhibits the mitochondrial respiratory chain to induce ROS formation and elicits apoptotic neuronal death⁸. In both animals and humans, MPTP administration specifically induced dopaminergic neuronal loss and provokes parkinsonian motor symptoms^{12–14}. One endogenous molecule thought to have similar cytotoxic properties to MPTP is DA itself. When free in the cytosol, DA auto-oxidation or its oxidation by the monoamine oxidase (MAO) results in ROS production, renders cells more vulnerable to other toxins^{15–17} and ultimately provokes apoptotic cell death^{18,19}.

The type-2 vesicular monoamine transporter (VMAT2), a neuronal H⁺-ATPase antiporter, is of particular interest when studying DA neurodegeneration given its protective role from endogenous and exogenous toxicants^{20,21}. The primary role of VMAT2 is to store monoamines into synaptic vesicles and to regulate stimulated monoamines quantal release^{22,23}, resulting in protection of monoamines from cytoplasmic oxidation. Indeed, by regulating the amount of DA accumulated in the cytosol, VMAT2 protects cells from their own neurotransmitter toxicity²⁴, suggesting that VMAT2 can modulate susceptibility of DA neurons to degeneration. Several different transgenic VMAT2 mice models have been developed to study the role of VMAT2 in monoaminergic signaling. The constitutive VMAT2 knockout (VMAT2-KO) mice, which die within few days after birth, displayed a 90–100% reduction in the total amount of monoamines in the entire brain confirming the impairment of monoamine storage and release induced by VMAT2 removal^{25–27}. Moreover, the constitutive VMAT2 heterozygote (VMAT2-HET) mice, viable into adulthood with a 30–40% decrease in brain monoamines level, showed increase vulnerability of DA neurons to both MPTP and L-DOPA toxicity^{26,28,29}. A recombinant event leading to the generation of a hypomorphic allele gave rise to VMAT2-knockdown (VMAT2-KD) mice which displays a 95% decrease in VMAT2 expression and function and have a 70%–90% decrease in brain monoamines. VMAT2-KD mice demonstrated an increase in DA- and MPTP-mediated toxicity that was sufficient to induce DA nigrostriatal pathway neurodegeneration^{29,30}. In human studies, VMAT2 gain of function haplotypes have been correlated with being protective for sporadic PD³¹. Moreover, DA uptake is reduced in PD patients suggesting that there may be an alteration of VMAT2 mediated vesicular filling in PD patients³².

Although current studies have outlined the relevance of VMAT2 in the understanding of PD pathogenesis neurodegeneration, VMAT2 deletion models lack specificity. Indeed, VMAT2-KO mice only survive for few days at birth^{25,27}, therefore making it difficult to evaluate the long term behavioral and pathological outcomes of a defect in VMAT2 expression. Although VMAT2-HET and VMAT2-KD mice are viable into adulthood, the deletions of VMAT2 expression are unspecific to the DA system and to the SN, inducing some secondary effects not relevant to PD.

The purpose of the present study is thus to analyze VMAT2's involvement in DA depletion-induced motor features associated with PD and examine the relevance of DA toxicity in the pathogenesis of neurodegeneration. We created viable VMAT2-KO mice specific to the DA nigrostriatal pathway; VMAT2 floxed engineered mice were stereotaxically injected in the SN with an adeno-associated virus (AAV) expressing the Cre-recombinase, allowing VMAT2 removal in DA neurons of the nigrostriatal pathway solely. In this model, DA depletion was observed exclusively in the dorsal striatum and was associated with motor deficits starting at 8 weeks post-injection ongoing until 16 and associated at this time with decreased food and water consumption, weight loss and accelerate death. However, during this time frame, these symptoms were not associated with any degeneration of nigrostriatal neurons. This study highlights a non-cytotoxic role of DA in our genetic model of VMAT2 deletion exclusively in nigrostriatal neurons, suggesting that preventing DA storage in vesicles and therefore DA release may not be responsible for the neurodegeneration seen in PD.

Results

Genetic, neurochemical and behavioral validation of specific ablation of the VMAT2 gene in the SN. Conditional ablation of the VMAT2 gene in the SN was obtained by injecting the AAV2 viral vector expressing the Cre recombinase, in the SN of 2 months old VMAT2^{lox/lox} mice. The Cre recombinase spliced out the VMAT2 floxed gene specifically in DA neurons of the SN.

To validate the specific conditional removal of VMAT2 in the SN, we assessed the efficiency of Cre-mediated splicing via radioactive VMAT2 *in situ* hybridization (Fig. 1A). A selective absence of VMAT2 mRNA labeling was observed in the SN starting at 8 weeks post-injection and ongoing, whereas VMAT2 mRNA was still expressed in DA neurons of the ventral tegmental area (VTA), demonstrating efficient and specific ablation of VMAT2 in the structure of interest.

The absence of VMAT2 mRNA observed in the SN of VMAT2^{lox/lox} injected with the AAV2 expressing the Cre recombinase was associated with a marked decrease in the tissue levels of DA in the dorsal striatum (Caudate Putamen, CPU), as measured via high performance liquid chromatography (HPLC) (Fig. 1B; Mann-Whitney U: AAV2-GFP vs AAV2-CRE-GFP: 8 weeks: U = 0, Z = 2.65, **p = 0.008; 16 weeks: U = 0, Z = 2.92, **p = 0.0034). In this same SN-projecting structure, the HVA:DA and DOPAC:DA ratios were increased in Cre-injected VMAT2^{lox/lox} mice compared with control mice (Fig. 1C; Mann-Whitney U: AAV2-GFP vs AAV2-CRE-GFP: HIAA/DA: U = 0, Z = -2.93, **p = 0.0034; DOPAC/DA: U = 6, Z = -2.07, *p = 0.038). This suggests that the amounts of DA was produced normally but quickly degraded due to the lack of VMAT2-dependent accumulation and protection in the vesicles. However, both DA level, HVA:DA and DOPAC:DA ratios were unchanged in the nucleus accumbens (NAc) and the prefrontal cortex (PFC), demonstrating DA nigrostriatal pathway specificity (Mann-Whitney U: AAV2-GFP vs AAV2-CRE-GFP: DA level: NAc - U = 12, Z = 1.21, p = 0.22; PFC - U = 15, Z = -0.78, p = 0.43; HVA/DA: NAc - U = 20, Z = 0.07, p = 0.94; PFC - U = 12, Z = -0.45, p = 0.65. DOPAC/DA: NAc - U = 17, Z = 0.5, p = 0.62; PFC - U = 14, Z = -0.091, p = 0.93).

After verifying specific ablation of VMAT2 in the SN associated with DA depletion in the dorsal striatum exclusively, we examined the consequences of unilateral DA depletion on rotational behavior. Unilateral injection

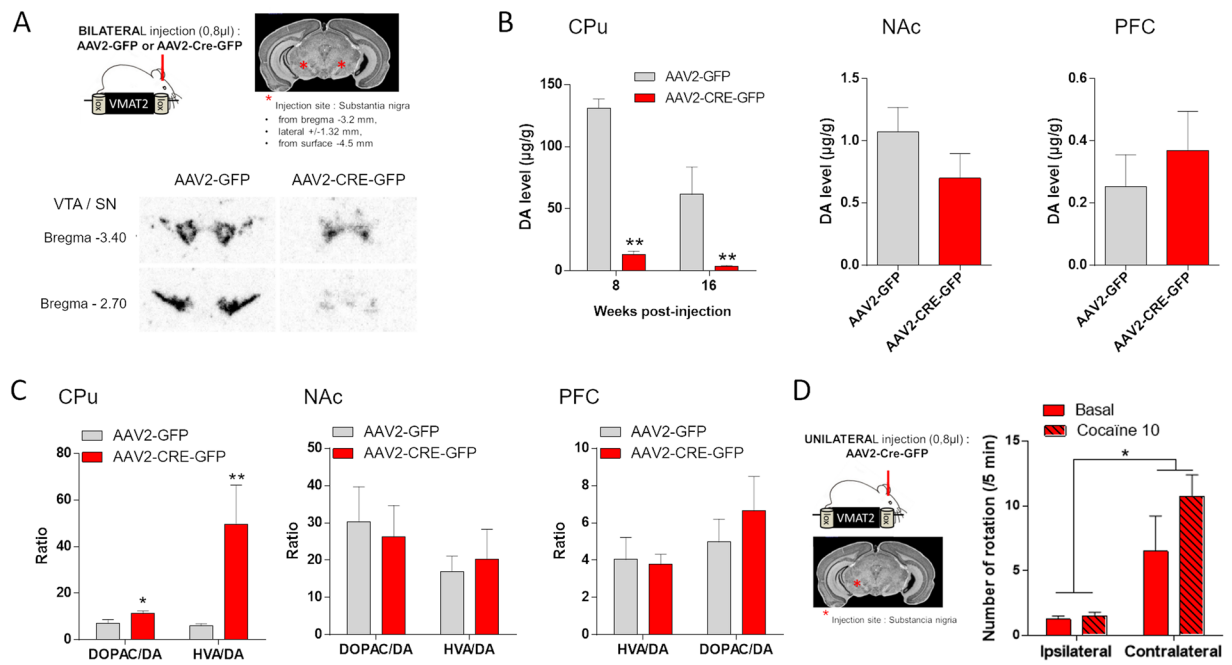


Figure 1. Genetic, neurochemical and behavioral validation of VMAT2 removal. **(A)** VMAT2 *in situ* hybridization in the SN and VTA of 2-month-old VMAT2^{lox/lox} mice injected bilaterally with AAV2-GFP or AAV2-CRE-GFP in the SN. **(B)** DA levels ($\mu\text{g/g}$ of protein) measured by HPLC in the CPu, NAc and PFC of VMAT2^{lox/lox} bilaterally injected with AAV2-GFP (8 weeks: $n = 5$; 16 weeks: $n = 6$) or AAV2-CRE-GFP (8 weeks: $n = 6$; 16 weeks: $n = 7$) in the SN at 8 and 16 weeks' post-injection (Mann-Whitney U: AAV2-GFP vs AAV2-CRE-GFP: 8 weeks: CPU $**p < 0.01$; 16 weeks: CPU $**p < 0.01$; NAc $p = 0.22$; PFC $p = 0.43$). **(C)** HVA/DA and DOPAC/DA ratio in the CPu, NAc and PFC at 16 weeks' post-injection of VMAT2^{lox/lox} mice bilaterally injected with AAV2-GFP ($n = 6$) or AAV2-CRE-GFP ($n = 7$) in the SN (Mann-Whitney U: AAV2-GFP vs AAV2-CRE-GFP: HIAA/DA: CPU $**p < 0.01$; NAc - $p = 0.28$; PFC - $p = 0.72$. DOPAC/DA: CPU $*p < 0.05$; NAc - $p = 0.62$; PFC $p = 0.83$). **(D)** Number of ipsilateral and contralateral rotations over 5 minutes in both basal condition and 10 minutes post-cocaine injection (10 mg/kg) in VMAT2^{lox/lox} mice AAV2-CRE unilaterally injected (16 weeks' post-injection, $n = 4$). (Wilcoxon test: ipsi vs contra: $*p < 0.05$). SN: Substantia nigra, VTA: Ventral Tegmental Area, CPu: Caudate Putamen, NAc: Nucleus Accumbens, PFC: PreFrontal Cortex, VMAT2: Vesicular Monoamine Transporter-2, AAV: Adenoassociated Virus, HVA: Homovanillic acid, DOPAC: 3,4-Dihydroxyphenylacetic acid.

of the cre-expressing viral vector in the SN of VMAT2^{lox/lox} mice led to contralateral rotations, an effect strengthened by 10 mg/kg cocaine injection (Fig. 1D; Wilcoxon test: ipsi vs contra $T = 0.00$, $Z = 2.52$; $*p = 0.012$).

Behavioral consequences of DA depletion in the nigrostriatal pathway. The survival curve of bilaterally Cre-injected VMAT2^{lox/lox} mice indicated a progressive decrease of the survival fraction of mice starting at 16 weeks post-injection with 100% of mice dead after 19 weeks whereas a survival rate of 100% was observed in control mice (Fig. 2A; Log-rank (Mantel-Cox) test: Chi square = 14.42, $p = 0.0001$). This effect on survival was associated with weight loss, at 16 weeks post-viral injection the weight of Cre-injected mice was 25.7 ± 1.5 g compared with 33.6 ± 1.9 for control mice (Fig. 2B; Mann-Whitney U: AAV2-GFP vs AAV2-CRE-GFP: Week 0: $U = 69.5$, $Z = 0.12$, $p = 0.91$; Week 4: $U = 69.5$, $Z = -0.12$, $p = 0.91$; Week 8: $U = 69$, $Z = -0.14$, $p = 0.88$; Week 12: $U = 58$, $Z = 0.78$, $p = 0.43$; Week 16: $U = 19$, $Z = 3.04$, $p = 0.002$). Food and water consumption of Cre-injected VMAT2^{lox/lox} mice compared with control was dramatically decreased at 16 weeks' post-injection (Mann-Whitney U: AAV2-GFP vs AAV2-CRE-GFP: Food consumption: $U = 6$, $Z = -2.14$, $*p = 0.032$; Water consumption: $U = 0.00$, $Z = -3.13$, $**p = 0.0017$), explaining weight lost and ultimately death (Fig. 2C).

Specific DA depletion in the nigrostriatal pathway induced motor ambulation and coordination alterations at 8 weeks' post-viral injection ongoing. The mean total distance travelled in an open field (Fig. 3A, Mann-Whitney U: AAV2-GFP vs AAV2-CRE-GFP: week 8 - $U = 6$, $Z = 2.37$, $p = 0.018$; week 12 - $U = 6$, $Z = 2.36$, $p = 0.018$; week 16 - $U = 9$, $Z = 1.98$, $p = 0.048$) and the latency to fall in the rotarod test (Fig. 3B, Mann-Whitney U: AAV2-GFP vs AAV2-CRE-GFP: week 8 - $U = 10$, $Z = 2.08$, $p = 0.037$; week 12 - $U = 9$, $Z = 2.20$, $p = 0.028$; week 16 - $U = 1$, $Z = 3.12$, $p = 0.0018$) were decreased in Cre-injected mice compared to control from week 8 post-injection and this decrease continued up to week 16. Moreover, while the mean total distance travelled was significantly decreased at week 16 compared to week 0 in Cre-injected mice (Fig. 3A, Friedman test: Chi Sqr_(7,4) = 16.45, $p = 0.0025$; Wilcoxon test: Week 0 vs week 16 $T = 1.00$, $Z = 2.19$, $*p = 0.028$), this effect was absent in control mice (Fig. 3A, Friedman test: Chi Sqr_(7,4) = 13.44, $p = 0.0093$; Wilcoxon test: Week 0 vs week 16 $T = 7.00$, $Z = 1.18$, $p = 0.24$). Similarly, in the rotarod accelerating test, a post-injection time effect was observed in the Cre-injected

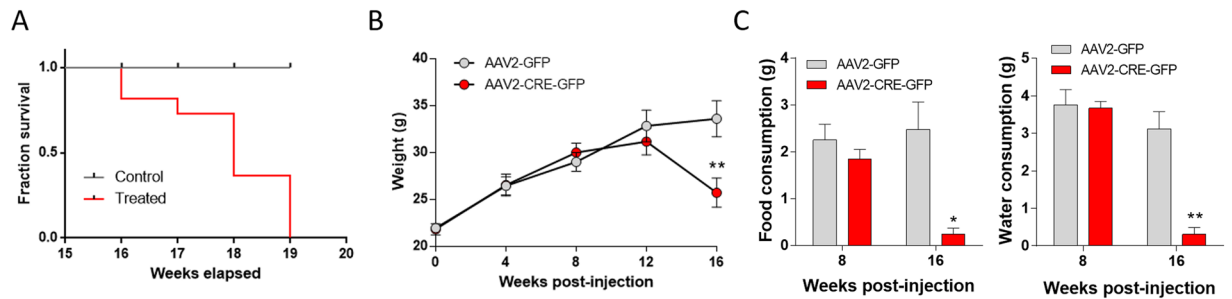


Figure 2. Survival, weight and food and water consumption. (A) Survival curve of VMAT2^{lox/lox} mice bilaterally injected with AAV2-GFP (n = 7) or AAV2-CRE-GFP (n = 8) in the SN (Log-rank (Mantel-Cox) test: $p < 0.001$). (B) Weight curve of VMAT2^{lox/lox} mice bilaterally injected with AAV2-GFP (n = 13) or AAV2-CRE-GFP (n = 11) in the SN (Mann-Whitney U: AAV2-GFP vs AAV2-CRE-GFP: Week 0: $p = 0.91$; Week 4: $p = 0.91$; Week 8: $p = 0.88$; Week 12: $p = 0.43$; Week 16: $**p < 0.01$). (C) Food and water consumption of VMAT2^{lox/lox} mice bilaterally injected with AAV2-GFP (n = 7) or AAV2-CRE-GFP (n = 7) in the SN at 8 and 16 weeks' post-virus injection (Mann-Whitney U: AAV2-GFP vs AAV2-CRE-GFP: Food consumption: Week 8: $p = 0.14$; Week 16: $*p < 0.05$; Water consumption: Week 8: $p = 0.53$; Week 16: $**p < 0.01$). SN: Substantia nigra, VMAT2: Vesicular Monoamine Transporter-2, AAV: Adenoassociated Virus.

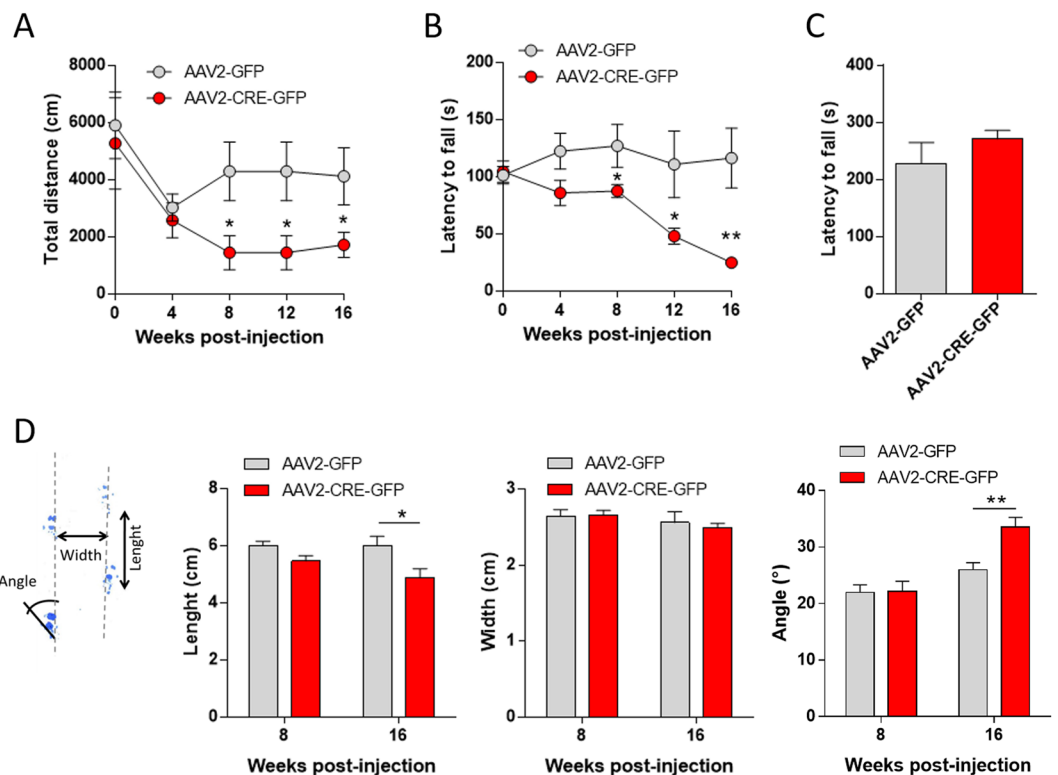


Figure 3. Motor behavioral consequences of nigrostriatal DA depletion. (A) Mean total distance (cm) measured at 5-min interval for 2 hrs every 4 weeks before and after AAV2-GFP or AAV2-CRE-GFP bilateral injection in VMAT2^{lox/lox} mice (n = 7 per groups; Mann-Whitney U: AAV2-GFP vs AAV2-CRE-GFP: week 8 to 16 $*p < 0.05$). (B) Mean latency to fall (s) in the accelerating rotarod over 4 consecutive sessions (4 to 25 rpm) every 4 weeks before and after AAV2-GFP (n = 8) or AAV2-CRE-GFP (n = 7) bilateral injection in VMAT2^{lox/lox} mice (Mann-Whitney U: AAV2-GFP vs AAV2-CRE-GFP: week 8 $*p < 0.05$; week 12 $*p < 0.05$; week 16 $**p < 0.01$). (C) Latency to fall (s) in the grip test 16 weeks' post-bilateral injection of AAV2-GFP or AAV2-CRE-GFP in VMAT2^{lox/lox} mice. Mann-Whitney U: AAV2-GFP vs AAV2-CRE-GFP: $p = 0.73$). (D) Gait analysis parameters in VMAT2^{lox/lox} mice 8 and 16 weeks' post AAV2-GFP or AAV2-CRE-GFP bilateral injection. Stride length (cm), stance width (cm) and paw angle ($^{\circ}$). No differences in gait at 8 weeks' post-injection (Mann-Whitney U: AAV2-GFP vs AAV2-CRE-GFP: Length $p = 0.11$; width $p = 0.90$; Angle $p = 0.93$). Change the coordination of ambulation in AAV2-CRE-GFP injected mice compared to AAV2-GFP at 16 weeks' post-injection (Mann-Whitney U: AAV2-GFP vs AAV2-CRE-GFP: Length $*p < 0.05$; width $p = 0.75$; Angle $**p < 0.01$). VMAT2: Vesicular Monoamine Transporter-2, AAV: Adenoassociated Virus.

mice (Fig. 3B, Friedman test: Chi Sqr_(7,4) = 22.74, $p = 0.00014$) indicating a decrease in performance over-time while no time effect was observed in the control mice (Fig. 3B, Friedman test: Chi Sqr_(8,4) = 2.9, $p = 0.57$).

However, the latency to fall in the grip test at 16 weeks' post-viral injection was unaltered in Cre-injected mice (Fig. 3C, Mann-Whitney U: AAV2-GFP vs AAV2-CRE-GFP: $U = 25$, $Z = -0.35$, $p = 0.73$). Finally, gait analysis indicated decreased in step length and angle whereas step width was unchanged, indicating change in the coordination of ambulation in AAV2-CRE-GFP injected mice compared to AAV2-GFP mice at 16 weeks' post-injection (Fig. 3D, Mann-Whitney U: AAV2-GFP vs AAV2-CRE-GFP: Length $U = 6$, $Z = -1.92$, $p = 0.054$; width $U = 16$, $Z = -0.32$, $p = 0.75$; Angle $U = 1$, $Z = 2.72$, $p = 0.0065$) with no changes at 8 weeks (Mann-Whitney U: AAV2-GFP vs AAV2-CRE-GFP: Length $U = 40$, $Z = -1.60$, $p = 0.11$; width $U = 64$, $Z = -0.12$, $p = 0.90$; Angle $U = 64$, $Z = -0.09$, $p = 0.93$).

Neuroanatomical consequences of DA depletion in the nigrostriatal pathway. To study whether DA depletion-induced motor alterations affected the neuroanatomical integrity of the nigrostriatal pathway, we looked at the expression of major DA markers.

DAT mRNA labeling measured by *in situ* hybridization were unchanged in the SN and the VTA of Cre-injected mice compared with controls (Fig. 4A, Mann-Whitney U: AAV2-GFP vs AAV2-CRE-GFP: SN - $U = 5$, $Z = -0.72$, $p = 0.47$; VTA - $U = 8$, $Z = 0.14$, $p = 0.14$), however, D2 mRNA labelling was increased in both the SN and the VTA of Cre-injected mice compared with control (Fig. 4B, Mann-Whitney U: AAV2-GFP vs AAV2-CRE-GFP: SN - $U = 0$, $Z = -2.16$, $p = 0.03$; VTA - $U = 0$, $Z = -2.16$, $p = 0.03$). Moreover, by performing TH immunostaining, we identified that the number of TH expressing neurons in the SN and in the VTA were identical between Cre-injected VMAT2^{lox/lox} mice and control mice (Fig. 4C,D, Mann-Whitney U: AAV2-GFP vs AAV2-CRE-GFP: SN - $U = 4$, $Z = -0.53$, $p = 0.59$; VTA - $U = 3$, $Z = -0.88$, $p = 0.38$). Finally, the density of TH positive fibers in both the CPu and the NAc was similar between both genotypes (Fig. 4C,D, Mann-Whitney U: AAV2-GFP vs AAV2-CRE-GFP: CPu - $U = 5$, $Z = 0.18$, $p = 0.86$; NAc - $U = 4$, $Z = 0.53$, $p = 0.6$). These results indicate that in our model of DA depletion with induced motor alterations, DA cytoplasmic accumulation due to the lack of VMAT2 expression is not sufficient to induced neurodegeneration.

Discussion

The present study directly addresses a role for the specific deficit of DA vesicular storage in the nigrostriatal pathway in the etiology of neuronal cell death in neurodegenerative disorders, and most particularly Parkinson disease. To reach this objective, we used a unique genetic model to remove in adult mice VMAT2 expression in DA neurons of the SN specifically. In conditional VMAT2 KO mice model, we previously showed that early somatic deletion of VMAT2 exclusively in DA neurons causes a rapid postnatal death³³, whereas the specific genetic deletion of VMAT2 in noradrenergic or serotonergic neurons does not prevent mice to live and grow up to adulthood³³⁻³⁵. This early postnatal death observed in conditional DA neurons-specific VMAT2 KO mice was similar to the one observed in constitutive VMAT2²⁵⁻²⁷ or DA-specific TH³⁶ KO mice. Therefore, to circumvent this limitation, we used floxed VMAT2 mice, that have no phenotypical alterations by themselves and we initiated the VMAT2 gene splicing by stereotaxic injection of a virus expressing the Cre-recombinase in adult mice.

It is well known that unilateral DA depletion induces rotational behavior, however the direction of the rotation is dependent upon the model or the drugs used. Contralateral rotational behavior is exhibited by 6-OHDA-lesioned rats, whereas ipsilateral rotations are produced in animals with electrolytic lesions³⁷. Moreover, in the 6OHDA model, while amphetamine induced ipsilateral rotation, contralateral rotation was observed with apomorphine³⁸. It has also been shown that activation of the direct pathway (D1) induced contralateral rotation in contrast to activation of the indirect pathway (D2) which induced ipsilateral rotation³⁹. In our model of genetic removal of VMAT2, unilateral injection of the Cre-expressing AAV2 in the SN shows the expected behavioral consequence of DA transmission imbalance; the contralateral rotations are of the same magnitude as those seen in unilateral 6-OHDA lesioned rats^{37,40,41}, and these spontaneous rotations are increased upon cocaine administration. Interestingly, despite that VMAT2 mRNA signal disappeared as early as 8 weeks after bilateral injection, we did not reliably observed these spontaneous rotations before 16 weeks following the viral administration. Accordingly, at 8 weeks following the bi-sided virus injections, DA levels are already significantly decreased by 90%, and the mice show significant locomotion and coordination deficits, but have a normal food and water intake and no weight loss. 16 weeks following viral administration in the SN, VMAT2^{lox/lox} AAV2cre injected mice showed a total collapse of DA tissue-concentration in the striatal target region, but not in the ventral striatum nor frontal cortex that are mostly innervated by DA fibers originating from the VTA⁴². At this time, when DA levels are as low as only 4–5% of the control, mice stop eating and drinking and all died within the next two weeks. We hypothesizes that the manifestation of contralateral rotational behavior, at 16 weeks post-virus injection, may suggest that the <5% remaining DA preferentially activate the direct pathway, as a consequence of DA higher affinity for the D1 DA receptor⁴³. Moreover, activation of the direct DA pathway is known to increase ambulation in mice³⁹. Acting preferentially on this pathway could be a compensatory mechanism to counteract the induced motor dysfunction. The absence of vesicular DA release is not paralleled by any anatomical alterations, as assessed by the key DA markers: the dopamine transporter (DAT), the D2 dopamine receptor and the tyrosine hydroxylase (TH) enzyme in cell-bodies and terminals. In contrast, an increase in D2 dopamine receptor mRNA is observed in the SN and the VTA of DA-depleted mice. This is in agreement with the absence of a role of DA in the development and maintenance of DA circuitry that have been observed in TH KO mice^{36,44}.

Vesicular transporters are mostly localized in nerve terminals, at distance from the cell body from where they have to be relocated, and this may advocate that they should have a quite robust maintenance giving their essential role in transmission⁴⁵⁻⁴⁷. However, at the present time and to our knowledge, we have absolutely no information regarding their half-life time, for any of them. Since the VMAT2-KD mice, expressing only 5% of VMAT2^{30,48}, survive for several months, we can infer that after 16 weeks, our dying VMAT2^{lox/lox}-cre mice must be below this

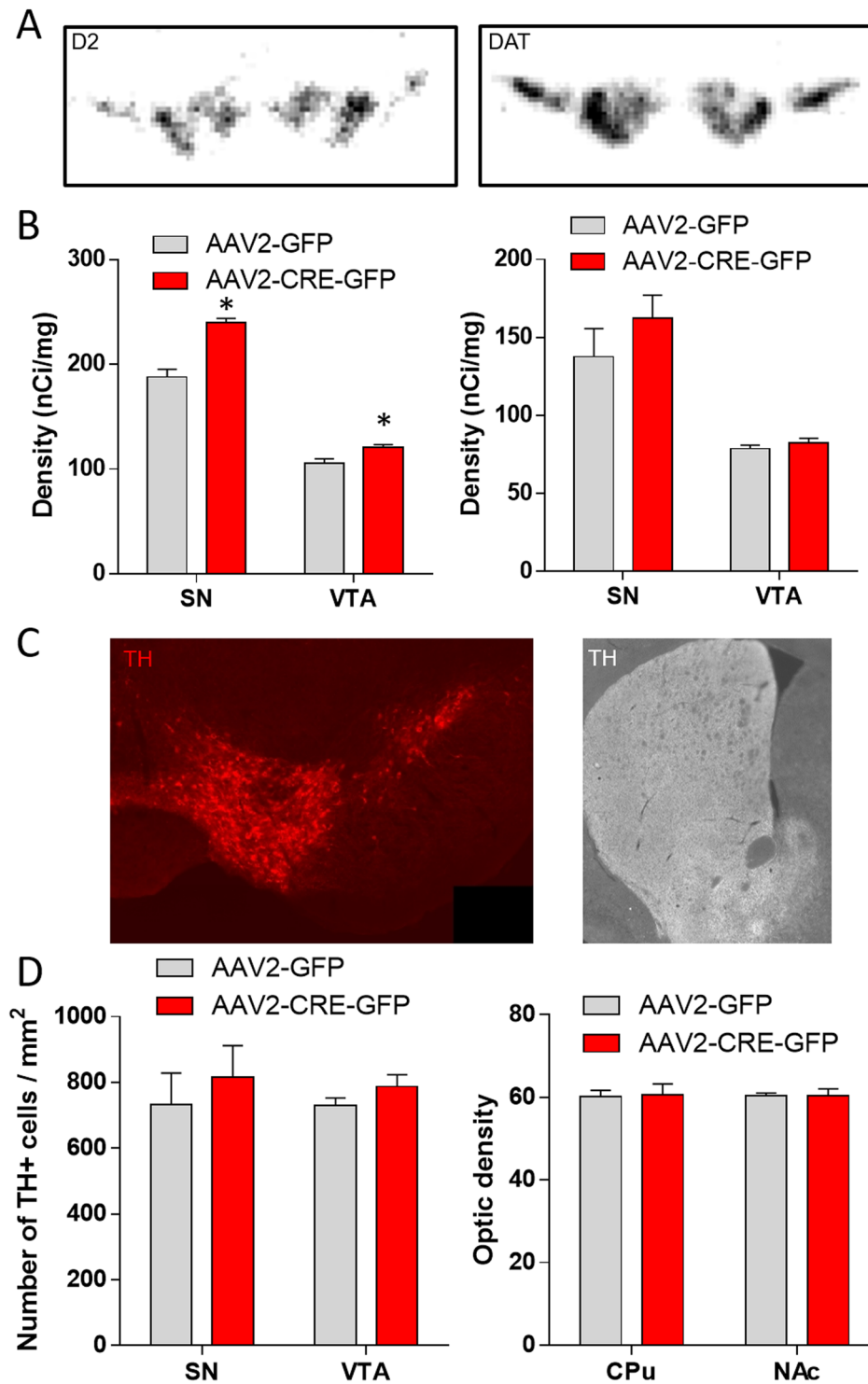


Figure 4. Neuroanatomical consequences of nigrostriatal DA depletion. (A) Illustration of D2 (left) and DAT (right) mRNA radioactive *in situ* labelling in the SN and the VTA. (B) Density (nCi/mg) of D2 (left) and DAT (right) mRNA expression in the SN and VTA, measured by radioactive *in situ* hybridization, 16-week after AAV2-GFP or AAV2-CRE-GFP bilateral injection in VMAT2^{lox/lox} mice (n = 4 per groups, Mann-Whitney U: AAV2-GFP vs AAV2-CRE-GFP: D2: SN *p < 0.05; VTA *p < 0.05; DAT: SN p = 0.47; VTA p = 0.14). (C) Illustration of TH immunostaining in DA neurons of the SN and the VTA (Left) and in the fibers in the CPu and NAc (Right). (D) Number of TH positive cell per mm² in the SN and the VTA (Left) and optic density of TH positive fibers in the CPu and the NAc (Right) 16-week after AAV2-GFP or AAV2-CRE-GFP bilateral injection in VMAT2^{lox/lox} mice (n = 4 per groups, Mann-Whitney U: AAV2-GFP vs AAV2-CRE-GFP: TH + cells: SN p = 0.59; VTA p = 0.38; optic density: CPu p = 0.86; NAc p = 0.6). SN: Substantia nigra, VTA: Ventral Tegmental Area, CPu: Caudate Putamen, NAc: Nucleus Accumbens, PFC: PreFrontal Cortex, VMAT2: Vesicular Monoamine Transporter-2, AAV: Adenoassociated Virus, TH: Tyrosine hydroxylase.

5% threshold of VMAT2 expression. Considering that it would take 5 half-life periods to reach 3.125% of expression and 6 half-time periods to reach 1.56%, and that mRNA depletion is reached in one week, it would imply that one half-life time period is comprised between 17.5 (15 Wk/6) and 21 (15 Wk/5) days. This value, that represents the first attempt to evaluate the life cycle of these transmembrane vesicular transporters, clearly indicates a very slow turnover rate and metabolism of this vesicular protein. Further experimental data, using complementary approaches, should now confirm this first report.

To evaluate a cytotoxic role for cytoplasmic DA, we tested the idea that the absence of DA-vesicular storage and the sequential increase of cytoplasmic DA may possibly trigger cell death through mitochondrial dysfunction and ROS generation^{49–52}. Supporting this hypothesis, a decrease of VMAT levels in Parkinson brains have been substantially found^{53–55}. However, our findings would indicate that it is more likely a consequence of DA neurons death, rather than a cause for their degeneration. We observed that, compared to 6-OHDA or MPTP lesions of the DA nuclei^{12–14} which induce a cellular death of DA neurons, the genetic deletion of VMAT2 we engineered here does not affect the anatomy of the DA system after 16 weeks, as observed by the absence of alteration in presynaptic markers of the dopaminergic system. The dopamine transporter (DAT) regulates extracellular DA level through reuptake of the release transmitter into presynaptic DA neurons. Tyrosine Hydroxylase (TH) is the rate-limiting enzyme in DA biosynthesis and its expression constitute a specific indicator of DA production^{56,57}. The D2 presynaptic auto-receptor regulates DA transmission by inhibiting the probability of vesicular DA release⁵⁸, decreasing DA synthesis⁵⁹ and altering the uptake of DA⁶⁰. Accordingly, DAT, the D2 presynaptic receptor and TH are the most appropriate markers of damage to the striatal DA terminals in PD^{61,62}. In our model, we did not find any alterations in DAT mRNA expression in the SN and TH immunoreactivity in both the striatum and the SN. These results are partially in accordance with the one observed in reserpine treated mice where no effect was found on DAT immunoreactivity but a decrease in striatum TH immunoreactivity was observed⁶³. However, transgenic mice expressing only 5% of VMAT2 (VMAT2-KD mice) present an age-dependent degeneration of nigrostriatal dopamine neurons. In this model of unspecific disruption of DA storage, mice exhibit decreased DAT and TH immunoreactivity in the striatum associated with increased oxidative damage³⁰. Finally, in our model of dopamine depletion, we find an increased expression of the D2 dopamine receptor mRNA in the SN and the VTA. In accordance with this effect, it was found that in mice lacking the dopamine transporter DAT, which display biochemical and behavioral dopaminergic hyperactivity, the D2 autoreceptors mRNA, measured by *in situ* hybridization is reduced in the ventral midbrain^{64,65}. In DAT-KO mice, this decrease was found mice to counteract the increased DA neurotransmission. In our experimental condition, we hypothesize that in absence of DA transmission, increased D2 autoreceptor expression may compensate the dramatic change in DA homeostasis.

Genetic and pharmacological reduction of VMAT2 resulted in lower tissue level of striatal DA. Consistently, in DA terminals of the striatum originating from the SN, we observed a dramatic collapse of DA concentration. As observed in VMAT2-KD mice, this reduction is accompanied by an increase in the ratios of DA metabolites to DA (HVA/DA and DOPAC/DA) suggesting an increase in DA turnover. This highlights that the genetically engineered deficit of DA storage, rather than uprising the accumulation of cytoplasmic DA, is accelerating the metabolic outcome of DA.

What is the actual value of animal models to assess the molecular and cellular etiology of PD? One good illustration of these timescale is by comparing the genetic deletion of the DAT in human and mice. In humans, mutations of the DAT gene is responsible for a very severe early onset of PD, which first motor symptoms usually appeared during the first postnatal year and young children are dying before the age of 10 years^{66–68}. In mice, the knockout of DAT does not trigger such a dramatic phenotype⁶⁴, even though it has been reported a sporadic death of about one third of DATKO mice, usually between the 20th and 50th postnatal week⁶⁹ when the mice where on a C57BL/6 background, whereas such high proportion of death is not seen when the DATKO mice are on a C57BL/6xDBAD/2 hybrid background⁷⁰. Actually, beside the neurotoxin-induced animal models, where DA neuronal death occurred quite rapidly, none of the genetic models of PD, based on gene inactivation or mutation, show any degeneration of DA neurons⁷¹. In our VMAT2 KO mice targeted to the SN, death occurred within 4 to 5 months, whereas in human, it takes decades for the catecholamines neurons to die upon the reaching of motor symptoms.

In summary, we engineered a new transgenic mice model of VMAT2 removal-induced DA depletion specifically in the nigrostriatal pathway. DA homeostasis alteration induced in this model reproduce motor deficit observed in PD, however, it is not sufficient to reveal DA cell loss and neurodegeneration characterizing PD physiopathology. Although this model of DA depletion does not fully recapitulate the complexity of the human disease, it constitutes the first model of dissociating DA depletion pathway. Here, we are able to target exclusively the nigrostriatal pathway without affecting the mesocorticolimbic pathway. This innovative model could help figure out the specific involvement of these two distinct DA pathways in both motor and non-motor function and dysfunction.

Methods

Animals. Animal housing, breeding, and care were operated in accordance to the Canadian Council on Animal Care guidelines (CCAC; http://ccac.ca/en/_standards/guidelines) and all methods were approved by the Animal Care Committee from the Douglas Institute Research Center under the protocol number 5570. All methods were performed in accordance with the relevant guidelines and regulations.

The mice were kept under standard conditions at 22 ± 1 °C, a 60% relative humidity, and a 12-h light-dark cycle with food and water available *ad libitum*.

The floxed VMAT2 mouse strain were obtained from the Mouse Clinical Institute (Institut Clinique de la Souris, MCI/ICS, Illkirch, France). Heterozygous VMAT2 floxed mice (VMAT2^{lox/+}) were crossed to generate homozygote mice (VMAT2^{lox/lox}) necessary for Cre-expressing viral vector injection. VMAT2^{lox/lox} mice were

maintained on a C57BL/6J background. After weaning and sexing, mice were housed in group of 4–5 animals per cage. Male VMAT^{lox/lox} mice were used for stereotaxic surgery at 2 months of age.

Stereotaxic surgery. Mice VMAT^{lox/lox} were anesthetized with isoflurane gas combined with oxygen, and placed onto the stereotaxic apparatus. Once the skull was exposed and a hole drilled bilaterally, the recombinant AAV2.CMV.HI.eGFP-Cre.WPRE.SV40 or control AAV2.CMV.PI.eGFP.WPRE.bGH virus vectors (Penn Vector Core, AV-2-PV2004 and AV-2-PV0101) were injected at a 0° angle into the SN (Anteroposterior from bregma: −3.2; Lateral from the midline: ± 1.32; Dorsoventral from the surface: −4.5). VMAT^{lox/lox} were randomly assigned to viral injection. Virus injections (0.5 µl per side at a rate of 0.05 µl/min) were done through an internal cannula connected via tubing to a 10-µl Hamilton micro syringes mounted on a micro-drive pump (WPI, Sarasota, FL, USA).

Quantitative *in situ* hybridization. At 8-week or 16-week post-stereotaxic injection, mice brains were collected after decapitation and frozen in isopentane at −30 °C. Brains were sliced in coronal sections (10 µm thick) using cryostat (Leica CM3050S) and rinsed in 0.1 M PBS, SSC 10 M and treated with 0.25% ethanol. [³⁵S]-dATP oligonucleotides (VMAT2: 5'-GAG GAA CAC GAT GAA CAG GAT CAG CTT GCG CGA GT-3'; 5'-CTA CGA CGG TGA GCA GCA TGT TGT CTA GCA GCA G-3'; D2: 5'-GTA GTT GTA GTG GGG CCT GTC TGG CTT CCC TTC G-3'; 5'-GGA CTG TCA GGG TTG CTA TGT AGA CCG TGG TGG G-3'; 5'-GTG AGC TGG TGG TGA CTG GGA GGG ATG GGG CTA TA-3'; 5'-GAA GGC GCT GTA GAG GACT GGT GGG ATG TTG CAG-3'; 5'-ACT CAG CAG TGC AGG ATC TTC ATG AAG GCC TTGC-3'; 5'-TCC TTC TGC TGG GAG AGC TTC CTG CGG CTC ATC GT-3'; 5'-GAT GAT AAA GAT GAG GAG GGT GAG CAG CAT GGC A-3'; DAT: 5'-GAC TTC CTG GGG TCT TCG TCT CTG CTC CCT CTA C-3'; 5'-GTA GGC CAG TTT CTC TCG AAA GGA CCC AGG CAG G-3'; 5'-GGT ATG CTC TGA TGC CGT CTA TGG CTC CAG GGA G-3'; 5'-GCC TGA GTG GCA GTA GCC TGA GCT GGT TTC AAG G-3'; 5'-GTT GGC CCA GTC GGG GAA GAT GTA GGC TCC GTA GT-3') were synthesized with terminal transferase (Amersham, Biosciences) to obtain a specific activity of 5 × 10⁸ dpm/µg. Sections were covered with 70 µl of hybridization mix and 5 × 10⁵ dpm of each labeled oligonucleotide, and incubated overnight at 42 °C in a humid chamber. Following washes and dehydration, slides were air-dried and exposed to a BAS-SR Fujifilm Imaging Plate for 5 days. The plates were scanned with a Fujifilm BioImaging Analyzer BAS-5000. Regions identification was based on Franklin and Paxinos Mouse Atlas²².

High Performance Liquid Chromatography. HPLC was performed on micropunches of 1 mm diameter from the dorsal striatum (CpU), the nucleus accumbens (NAc), and the prefrontal cortex (PFC) of VMAT^{lox/lox} at 8 and 16 weeks post viral injection. After decapitation, brains were collected, frozen in isopentane at −30 °C and stored at −80 °C. Micropunches of specific structures were homogenized in a solution containing 45 µl of 0.25 M perchlorate and 15 µl of DHBA (100 mg/ml) which served as an internal standard. Following centrifugation at 10,000 rpm for 15 minutes at 4 °C, the supernatant was isolated to detect DA, dihydroxyphenylacetic acid (DOPAC), homovanillic acid (HVA), NE, serotonin (5-HT), and 5-hydroxyindolacetic acid (HIAA) using high pressure liquid chromatography with electrochemical detection (HPLC-EC). Samples were run through a Luna C18 (2) 75 × 4.6 mm 3 µm analytical column at a flow rate of 1.5 ml/min and the electrochemical detector (ESA Coullarray, model #5600 A) was set at a potential of −250 mV and +300 mV. The mobile phase consisted of 6% methanol, 0.341 mM 1-octanesulfoic acid sodium salt, 168.2 mM sodium acetate, 66.6 mM citric acid monohydrate, 0.025 mM ethylenediamine-tetra-acetic acid disodium (EDTA) and 0.71 mM triethylamine adjusted to pH 4.0–4.1 with acetic acid. Using ESA's CoullArray software, the position of the peaks for each metabolite was compared to an external standard solution containing 25 ng/ml DHBA, DA, NE, 5-HT, DOPAC, HVA, and 50 mM acetic acid. In parallel, pellets were reconstituted in 50 µl of 0.1 N NaOH and kept for protein quantification using a BCATM Protein Assay Kit (Fisher Scientific, Ontario, Canada). Each analyzed sample was measured in µg/g of protein.

Immunofluorescence labeling. Mice were perfused with 0.9% NaCl followed by 4% paraformaldehyde (PFA). Brains were collected and post-fixed in 4% PFA for 2 hours, and kept in a 15% sucrose solution at 4 °C before being sliced in coronal sections (40 µm thick) using a cryostat (Leica CM3050S). Free-floating slices of VMAT^{lox/lox} mice injected with the AAV2-GFP or the AAV2-CRE-GFP into the SN were rinsed in PBS 0.1 M and incubated overnight with a rabbit anti-TH (1/4000; Santa Cruz, sc-14007) primary antibody diluted in PBS 0.1 M, 2% normal goat serum (NGS), and 0.3% triton. After washes, slices were incubated for 2 hours in secondary antibody, a goat anti-rabbit alexa 555 (1/500; Life technologies, A-21429) diluted in PBS 0.1 M with 2% NGS, and 0.3% triton. Sections were then rinsed and mounted onto gelatin-coated slides under Vectashield mounting medium.

The number of TH expressing cells in the SN and the VTA was counted bilaterally on every three sections (total of 6 sections per animal) throughout the entire nucleus from bregma −2.70 to bregma −3.88. The density of TH positive fibers was analyzed bilaterally on every three slices for a total of seven sections per animal throughout the NAc from bregma −1.70 to bregma 0.74 and on nine sections throughout the CPu from bregma −1.70 to bregma 0.14.

Spontaneous and evoked rotations. At 16 weeks' post unilateral viral injection in the SN, VMAT2^{lox/lox} mice were placed in a cylindrical open field (40 cm diameter). Ipsilateral and contralateral rotation, defined as each 360° rotations that contain no turn of more than 90° in the opposite direction, were recorded during 5 minutes in baseline conditions and after cocaine injection (10 mg/kg, recording started 10 minutes after injections). Cocaine hydrochloride (Sigma Aldrich) diluted in a NaCl 0.9% was administrated intraperitoneally.

Locomotor activity and motor coordination. Spontaneous locomotion was measured before the viral injection and every 4 weeks after the viral injection in an Omnitech digiscan activity monitor. Plexiglas open-field chambers (40 cm²) with photocells placed on bottom and lateral surfaces allowed to measure the total distance travelled at 5-minute intervals for 2 hours.

Motor coordination was assessed by an accelerating rotarod (ROTO-ROD, Series 8, IITC Life Sciences) before the viral injections and every 4 weeks after the viral injection. The mice latency to fall was recorded over 4 consecutive trials at a rotating speed range from 4 to 25 accelerating rpm for a maximum of 5 minutes.

Gait analysis. At 8 and 16 weeks' post-viral injection, the gait of VMAT2^{lox/lox} mouse during spontaneous walk/trot locomotion was analyzed to identify specific paw step (stride length; stride width, and stride angle).

Grip test. 16 weeks post viral injection, VMAT^{lox/lox} mice were placed in the center of the wire mesh screen (12 mm squares of 1 mm diameter wir) and the screen were rotated to an inverted position over 2 sec, with the mouse's head declining first. The screen was held steadily 40–50 cm above a padded surface. The time when the mouse falls off was recorded, or it was removed when the criterion time of 300 sec was reached.

Statistical analysis. The results are expressed as mean ± SEM (standard error of the mean). No statistical methods were used to pre-determine sample sizes, but our sample sizes were similar to those generally employed in literature for the same paradigms. Statistical analyses were performed using Statistica software. Since the sample sizes were small ($n < 30$) and/or the variables did not follow a normal distribution (Shapiro–Wilk test) and/or the variances were not equal among groups (Leven test), we used a nonparametric statistical analysis. For 2 × 2 comparisons, we performed the Mann–Whitney *U* test for two independent samples (AAV2-GFP vs AAV2-CRE-GFP) and the Wilcoxon matched pairs test for dependent samples (8 weeks vs 16 weeks; Ipsilateral vs contralateral). For multiple repeated measures analysis (Total distance travelled and latency to fall in the rotarod), we used the Friedman test followed by the Wilcoxon test for the 2 × 2 comparisons. The comparison of the survival distribution between AVV2-GFP and AAV2-CRE-GFP groups was analyzed using the log-rank (Mantel-cox) test. Optic density was quantified using MCID for VMAT2, D2 and DAT mRNA labelling and the number of TH positive fibres in the striatum (CPU vs NAC) with image J. A *P* value < 0.05 was taken to indicate statistical significant differences between groups.

References

- de Lau, L. M. & Breteler, M. M. Epidemiology of Parkinson's disease. *The Lancet. Neurology* **5**, 525–535, [https://doi.org/10.1016/S1474-4422\(06\)70471-9](https://doi.org/10.1016/S1474-4422(06)70471-9) (2006).
- Forno, L. S. Neuropathology of Parkinson's disease. *Journal of neuropathology and experimental neurology* **55**, 259–272 (1996).
- Jankovic, J. Parkinson's disease: clinical features and diagnosis. *Journal of neurology, neurosurgery, and psychiatry* **79**, 368–376, <https://doi.org/10.1136/jnnp.2007.131045> (2008).
- Bohnen, N. I. *et al.* Positron emission tomography of monoaminergic vesicular binding in aging and Parkinson disease. *Journal of cerebral blood flow and metabolism: official journal of the International Society of Cerebral Blood Flow and Metabolism* **26**, 1198–1212, <https://doi.org/10.1038/sj.jcbfm.9600276> (2006).
- Ehringer, H. & Hornykiewicz, O. [Distribution of noradrenaline and dopamine (3-hydroxytyramine) in the human brain and their behavior in diseases of the extrapyramidal system]. *Klinische Wochenschrift* **38**, 1236–1239 (1960).
- Greffard, S. *et al.* Motor score of the Unified Parkinson Disease Rating Scale as a good predictor of Lewy body-associated neuronal loss in the substantia nigra. *Archives of neurology* **63**, 584–588, <https://doi.org/10.1001/archneur.63.4.584> (2006).
- Hilker, R. *et al.* Dementia in Parkinson disease: functional imaging of cholinergic and dopaminergic pathways. *Neurology* **65**, 1716–1722, <https://doi.org/10.1212/01.wnl.0000191154.78131.f6> (2005).
- Jenner, P. Oxidative stress in Parkinson's disease. *Annals of neurology* **53** (Suppl 3), S26–36; discussion S36–28, doi:<https://doi.org/10.1002/ana.10483> (2003).
- Jenner, P., Dexter, D. T., Sian, J., Schapira, A. H. & Marsden, C. D. Oxidative stress as a cause of nigral cell death in Parkinson's disease and incidental Lewy body disease. The Royal Kings and Queens Parkinson's Disease Research Group. *Annals of neurology* **32**(Suppl), S82–87 (1992).
- Jenner, P. & Olanow, C. W. Oxidative stress and the pathogenesis of Parkinson's disease. *Neurology* **47**, S161–170 (1996).
- Sanders, L. H. & Greenamyre, J. T. Oxidative damage to macromolecules in human Parkinson disease and the rotenone model. *Free radical biology & medicine* **62**, 111–120, <https://doi.org/10.1016/j.freeradbiomed.2013.01.003> (2013).
- Langston, J. W. & Ballard, P. Parkinsonism induced by 1-methyl-4-phenyl-1,2,3,6-tetrahydropyridine (MPTP): implications for treatment and the pathogenesis of Parkinson's disease. *The Canadian journal of neurological sciences. Le journal canadien des sciences neurologiques* **11**, 160–165 (1984).
- Langston, J. W. & Ballard, P. A. Jr. Parkinson's disease in a chemist working with 1-methyl-4-phenyl-1,2,5,6-tetrahydropyridine. *The New England journal of medicine* **309**, 310 (1983).
- Ricaurte, G. A. *et al.* Fate of nigrostriatal neurons in young mature mice given 1-methyl-4-phenyl-1,2,3,6-tetrahydropyridine: a neurochemical and morphological reassessment. *Brain research* **376**, 117–124 (1986).
- Barzilai, A., Melamed, E. & Shirvan, A. Is there a rationale for neuroprotection against dopamine toxicity in Parkinson's disease? *Cellular and molecular neurobiology* **21**, 215–235 (2001).
- Choi, D. K. *et al.* Ablation of the inflammatory enzyme myeloperoxidase mitigates features of Parkinson's disease in mice. *The Journal of neuroscience: the official journal of the Society for Neuroscience* **25**, 6594–6600, <https://doi.org/10.1523/JNEUROSCI.0970-05.2005> (2005).
- Cohen, G. & Spina, M. B. Deprenyl suppresses the oxidant stress associated with increased dopamine turnover. *Annals of neurology* **26**, 689–690, <https://doi.org/10.1002/ana.410260518> (1989).
- Ziv, I. *et al.* Dopamine induces apoptosis-like cell death in cultured chick sympathetic neurons—a possible novel pathogenetic mechanism in Parkinson's disease. *Neuroscience letters* **170**, 136–140 (1994).
- Ziv, I., Shirvan, A., Offen, D., Barzilai, A. & Melamed, E. Molecular biology of dopamine-induced apoptosis: possible implications for Parkinson's disease. *Methods in molecular medicine* **62**, 73–87, <https://doi.org/10.1385/1-59259-142-6:73> (2001).
- Guillot, T. S. & Miller, G. W. Protective actions of the vesicular monoamine transporter 2 (VMAT2) in monoaminergic neurons. *Molecular neurobiology* **39**, 149–170, <https://doi.org/10.1007/s12035-009-8059-y> (2009).
- Liu, Y. *et al.* A cDNA that suppresses MPP+ toxicity encodes a vesicular amine transporter. *Cell* **70**, 539–551 (1992).
- Henry, J. P. *et al.* Biochemistry and molecular biology of the vesicular monoamine transporter from chromaffin granules. *The Journal of experimental biology* **196**, 251–262 (1994).

23. Pothos, E. N. *et al.* Synaptic vesicle transporter expression regulates vesicle phenotype and quantal size. *The Journal of neuroscience: the official journal of the Society for Neuroscience* **20**, 7297–7306 (2000).
24. Uhl, G. R. Hypothesis: the role of dopaminergic transporters in selective vulnerability of cells in Parkinson's disease. *Annals of neurology* **43**, 555–560, <https://doi.org/10.1002/ana.410430503> (1998).
25. Fon, E. A. *et al.* Vesicular transport regulates monoamine storage and release but is not essential for amphetamine action. *Neuron* **19**, 1271–1283 (1997).
26. Takahashi, N. *et al.* VMAT2 knockout mice: heterozygotes display reduced amphetamine-conditioned reward, enhanced amphetamine locomotion, and enhanced MPTP toxicity. *Proceedings of the National Academy of Sciences of the United States of America* **94**, 9938–9943 (1997).
27. Wang, Y. M. *et al.* Knockout of the vesicular monoamine transporter 2 gene results in neonatal death and supersensitivity to cocaine and amphetamine. *Neuron* **19**, 1285–1296 (1997).
28. Kariya, S., Takahashi, N., Hirano, M. & Ueno, S. Increased vulnerability to L-DOPA toxicity in dopaminergic neurons from VMAT2 heterozygote knockout mice. *Journal of molecular neuroscience: MN* **27**, 277–279, <https://doi.org/10.1385/JMN:27:3:277> (2005).
29. Lohr, K. M. *et al.* Vesicular Monoamine Transporter 2 (VMAT2) Level Regulates MPTP Vulnerability and Clearance of Excess Dopamine in Mouse Striatal Terminals. *Toxicological sciences: an official journal of the Society of Toxicology* **153**, 79–88, <https://doi.org/10.1093/toxsci/kfw106> (2016).
30. Caudle, W. M. *et al.* Reduced vesicular storage of dopamine causes progressive nigrostriatal neurodegeneration. *The Journal of neuroscience: the official journal of the Society for Neuroscience* **27**, 8138–8148, <https://doi.org/10.1523/JNEUROSCI.0319-07.2007> (2007).
31. Glatt, C. E., Wahner, A. D., White, D. J., Ruiz-Linares, A. & Ritz, B. Gain-of-function haplotypes in the vesicular monoamine transporter promoter are protective for Parkinson disease in women. *Human molecular genetics* **15**, 299–305, <https://doi.org/10.1093/hmg/ddi445> (2006).
32. Pifl, C. *et al.* Is Parkinson's disease a vesicular dopamine storage disorder? Evidence from a study in isolated synaptic vesicles of human and nonhuman primate striatum. *The Journal of neuroscience: the official journal of the Society for Neuroscience* **34**, 8210–8218, <https://doi.org/10.1523/JNEUROSCI.5456-13.2014> (2014).
33. Isingrini, E. *et al.* Selective genetic disruption of dopaminergic, serotonergic and noradrenergic neurotransmission: insights into motor, emotional and addictive behaviour. *Journal of psychiatry & neuroscience: JPN* **41**, 169–181 (2016).
34. Isingrini, E. *et al.* Resilience to chronic stress is mediated by noradrenergic regulation of dopamine neurons. *Nature neuroscience* **19**, 560–563, <https://doi.org/10.1038/nn.4245> (2016).
35. Narboux-Neme, N. *et al.* Severe serotonin depletion after conditional deletion of the vesicular monoamine transporter 2 gene in serotonin neurons: neural and behavioral consequences. *Neuropsychopharmacology: official publication of the American College of Neuropsychopharmacology* **36**, 2538–2550, <https://doi.org/10.1038/npp.2011.142> (2011).
36. Zhou, Q. Y. & Palmiter, R. D. Dopamine-deficient mice are severely hypoactive, adipsic, and aphagic. *Cell* **83**, 1197–1209 (1995).
37. Iwamoto, E. T., Loh, H. H. & Way, E. L. Circling behavior in rats with 6-hydroxydopamine or electrolytic nigral lesions. *European journal of pharmacology* **37**, 339–356 (1976).
38. Kirik, D., Rosenblad, C. & Bjorklund, A. Characterization of behavioral and neurodegenerative changes following partial lesions of the nigrostriatal dopamine system induced by intra-striatal 6-hydroxydopamine in the rat. *Experimental neurology* **152**, 259–277, <https://doi.org/10.1006/exnr.1998.6848> (1998).
39. Kravitz, A. V. *et al.* Regulation of parkinsonian motor behaviours by optogenetic control of basal ganglia circuitry. *Nature* **466**, 622–626, <https://doi.org/10.1038/nature09159> (2010).
40. Fuxe, K. & Ungerstedt, U. Antiparkinsonian drugs and dopaminergic neostriatal mechanisms: studies in rats with unilateral 6-hydroxydopamine (=6-OH-DA)-induced degeneration of the nigro-neostriatal DA pathway and quantitative recording of rotational behaviour. *Pharmacology & therapeutics. Part B: General & systematic pharmacology* **2**, 41–47 (1976).
41. Ungerstedt, U. 6-hydroxydopamine-induced degeneration of the nigrostriatal dopamine pathway: the turning syndrome. *Pharmacology & therapeutics. Part B: General & systematic pharmacology* **2**, 37–40 (1976).
42. Bjorklund, A. & Dunnett, S. B. Dopamine neuron systems in the brain: an update. *Trends in neurosciences* **30**, 194–202, <https://doi.org/10.1016/j.tins.2007.03.006> (2007).
43. Seeman, P. & Van Tol, H. H. Dopamine receptor pharmacology. *Trends in pharmacological sciences* **15**, 264–270 (1994).
44. Zhou, Q. Y., Quafe, C. J. & Palmiter, R. D. Targeted disruption of the tyrosine hydroxylase gene reveals that catecholamines are required for mouse fetal development. *Nature* **374**, 640–643, <https://doi.org/10.1038/374640a0> (1995).
45. Fei, H., Grygoruk, A., Brooks, E. S., Chen, A. & Krantz, D. E. Trafficking of vesicular neurotransmitter transporters. *Traffic* **9**, 1425–1436, <https://doi.org/10.1111/j.1600-0854.2008.00771.x> (2008).
46. Edwards, R. H. The transport of neurotransmitters into synaptic vesicles. *Current opinion in neurobiology* **2**, 586–594 (1992).
47. Edwards, R. H. The neurotransmitter cycle and quantal size. *Neuron* **55**, 835–858, <https://doi.org/10.1016/j.neuron.2007.09.001> (2007).
48. Mooslehner, K. A. *et al.* Mice with very low expression of the vesicular monoamine transporter 2 gene survive into adulthood: potential mouse model for parkinsonism. *Molecular and cellular biology* **21**, 5321–5331, <https://doi.org/10.1128/MCB.21.16.5321-5331.2001> (2001).
49. Bose, A. & Beal, M. F. Mitochondrial dysfunction in Parkinson's disease. *Journal of neurochemistry* **139**(Suppl 1), 216–231, <https://doi.org/10.1111/jnc.13731> (2016).
50. Berman, S. B. & Hastings, T. G. Dopamine oxidation alters mitochondrial respiration and induces permeability transition in brain mitochondria: implications for Parkinson's disease. *Journal of neurochemistry* **73**, 1127–1137 (1999).
51. Lin, M. T. & Beal, M. F. Mitochondrial dysfunction and oxidative stress in neurodegenerative diseases. *Nature* **443**, 787–795, <https://doi.org/10.1038/nature05292> (2006).
52. Blesa, J., Trigo-Damas, I., Quiroga-Varela, A. & Jackson-Lewis, V. R. Oxidative stress and Parkinson's disease. *Frontiers in neuroanatomy* **9**, 91, <https://doi.org/10.3389/fnana.2015.00091> (2015).
53. Miller, G. W. *et al.* Immunohistochemical analysis of vesicular monoamine transporter (VMAT2) protein in Parkinson's disease. *Experimental neurology* **156**, 138–148, <https://doi.org/10.1006/exnr.1998.7008> (1999).
54. Thibaut, F. *et al.* Regional distribution of monoamine vesicular uptake sites in the mesencephalon of control subjects and patients with Parkinson's disease: a postmortem study using tritiated tetraabenazine. *Brain research* **692**, 233–243 (1995).
55. Goldstein, D. S. *et al.* Deficient vesicular storage: A common theme in catecholaminergic neurodegeneration. *Parkinsonism & related disorders* **21**, 1013–1022, <https://doi.org/10.1016/j.parkreldis.2015.07.009> (2015).
56. Goldstein, M. Regulatory mechanisms of dopamine biosynthesis at the tyrosine hydroxylase step. *Annals of the New York Academy of Sciences* **430**, 1–5 (1984).
57. Levitt, M., Spector, S., Sjoerdsma, A. & Udenfriend, S. Elucidation of the Rate-Limiting Step in Norepinephrine Biosynthesis in the Perfused Guinea-Pig Heart. *The Journal of pharmacology and experimental therapeutics* **148**, 1–8 (1965).
58. Phillips, P. E., Hancock, P. J. & Stamford, J. A. Time window of autoreceptor-mediated inhibition of limbic and striatal dopamine release. *Synapse* **44**, 15–22, <https://doi.org/10.1002/syn.10049> (2002).
59. Wolf, M. E. & Roth, R. H. Autoreceptor regulation of dopamine synthesis. *Annals of the New York Academy of Sciences* **604**, 323–343 (1990).

60. Truong, J. G., Newman, A. H., Hanson, G. R. & Fleckenstein, A. E. Dopamine D2 receptor activation increases vesicular dopamine uptake and redistributes vesicular monoamine transporter-2 protein. *European journal of pharmacology* **504**, 27–32, <https://doi.org/10.1016/j.ejphar.2004.09.049> (2004).
61. Miller, G. W. *et al.* Immunochemical analysis of dopamine transporter protein in Parkinson's disease. *Annals of neurology* **41**, 530–539, <https://doi.org/10.1002/ana.410410417> (1997).
62. Olanow, C. W. & Tatton, W. G. Etiology and pathogenesis of Parkinson's disease. *Annual review of neuroscience* **22**, 123–144, <https://doi.org/10.1146/annurev.neuro.22.1.123> (1999).
63. de Freitas, C. M. *et al.* Behavioral and neurochemical effects induced by reserpine in mice. *Psychopharmacology* **233**, 457–467, <https://doi.org/10.1007/s00213-015-4118-4> (2016).
64. Giros, B., Jaber, M., Jones, S. R., Wightman, R. M. & Caron, M. G. Hyperlocomotion and indifference to cocaine and amphetamine in mice lacking the dopamine transporter. *Nature* **379**, 606–612, <https://doi.org/10.1038/379606a0> (1996).
65. Jaber, M. *et al.* Differential regulation of tyrosine hydroxylase in the basal ganglia of mice lacking the dopamine transporter. *The European journal of neuroscience* **11**, 3499–3511 (1999).
66. Assmann, B. E. *et al.* Infantile Parkinsonism-dystonia and elevated dopamine metabolites in CSF. *Neurology* **62**, 1872–1874 (2004).
67. Kurian, M. A. *et al.* Homozygous loss-of-function mutations in the gene encoding the dopamine transporter are associated with infantile parkinsonism-dystonia. *The Journal of clinical investigation* **119**, 1595–1603, <https://doi.org/10.1172/JCI39060> (2009).
68. Kurian, M. A. *et al.* Clinical and molecular characterisation of hereditary dopamine transporter deficiency syndrome: an observational cohort and experimental study. *The Lancet. Neurology* **10**, 54–62, [https://doi.org/10.1016/S1474-4422\(10\)70269-6](https://doi.org/10.1016/S1474-4422(10)70269-6) (2011).
69. Cyr, M. *et al.* Sustained elevation of extracellular dopamine causes motor dysfunction and selective degeneration of striatal GABAergic neurons. *Proceedings of the National Academy of Sciences of the United States of America* **100**, 11035–11040, <https://doi.org/10.1073/pnas.1831768100> (2003).
70. Morice, E., Denis, C., Giros, B. & Nosten-Bertrand, M. Phenotypic expression of the targeted null-mutation in the dopamine transporter gene varies as a function of the genetic background. *The European journal of neuroscience* **20**, 120–126, <https://doi.org/10.1111/j.1460-9568.2004.03465.x> (2004).
71. Blesa, J. & Przedborski, S. Parkinson's disease: animal models and dopaminergic cell vulnerability. *Frontiers in neuroanatomy* **8**, 155, <https://doi.org/10.3389/fnana.2014.00155> (2014).

Acknowledgements

B. Giros is a Canadian Research Chair in the Neurobiology of Mental Disorders. E. Isingrini was supported by a postdoctoral grant from the FRQS. This work was supported by the Canada Research Chairs program, the Graham Boeckh Foundation for Schizophrenia Research and the Natural and Engineering Research Council of Canada (RGPIN 385732-2012) to B.G. We thank E. Vigneault and M.E. Desaulniers for excellent care and maintenance of all mice colonies.

Author Contributions

The studies were conceived and designed by B.G. with E.I. Experiments were performed by E.I. with the contribution of L.P. and Q.R. for mice experiments, C.G. for *in situ* analysis and immunohistochemistry, A.G. and L.M. for the neurochemical analysis. The paper was written by B.G., E.I. and C.G. and was edited by the other authors.

Additional Information

Competing Interests: The authors declare that they have no competing interests.

Publisher's note: Springer Nature remains neutral with regard to jurisdictional claims in published maps and institutional affiliations.



Open Access This article is licensed under a Creative Commons Attribution 4.0 International License, which permits use, sharing, adaptation, distribution and reproduction in any medium or format, as long as you give appropriate credit to the original author(s) and the source, provide a link to the Creative Commons license, and indicate if changes were made. The images or other third party material in this article are included in the article's Creative Commons license, unless indicated otherwise in a credit line to the material. If material is not included in the article's Creative Commons license and your intended use is not permitted by statutory regulation or exceeds the permitted use, you will need to obtain permission directly from the copyright holder. To view a copy of this license, visit <http://creativecommons.org/licenses/by/4.0/>.

© The Author(s) 2017